JOC The Journal of Organic Chemistry

Article

pubs.acs.org/joc

Influence of Solvation and Dynamics on the Mechanism and Kinetics of Nucleophilic Aromatic Substitution Reactions in Liquid Ammonia

Samuel L. C. Moors,*[,†] Ben Brigou,[†] Dietmar Hertsen,[‡] Balazs Pinter,[†] Paul Geerlings,[†] Veronique Van Speybroeck,[‡] Saron Catak,[§] and Frank De Proft[†]

[†]Eenheid Algemene Chemie (ALGC), Vrije Universiteit Brussel (VUB), Pleinlaan 2, 1050 Elsene, Brussels, Belgium

[‡]Center for Molecular Modeling (CMM), Ghent University, Technologiepark 903, 9052 Zwijnaarde, Belgium

[§]Department of Chemistry, Bogazici University, Bebek 34342, Istanbul, Turkey

Supporting Information

ABSTRACT: The role of the solvent and the influence of dynamics on the kinetics and mechanism of the S_NAr reaction of several halonitrobenzenes in liquid ammonia, using both static calculations and dynamic ab initio molecular dynamics simulations, are investigated. A combination of metadynamics and committor analysis methods reveals how this reaction can change from a concerted, one-step mechanism in gas phase to a stepwise pathway, involving a metastable Meisenheimer complex, in liquid ammonia. This clearly establishes, among others, the important role of the solvent and highlights the fact that accurately treating solvation is of crucial importance to correctly unravel the reaction mechanism. It is indeed shown that H-bond formation of the reacting NH_3 with the solvent drastically reduces the barrier of NH_3 addition. The halide elimination step, however, is greatly facilitated by proton transfer from the reacting NH_3 to the solvent. Furthermore, the free energy surface strongly depends on the halide substituent and the number of electron-withdrawing nitro substituents.

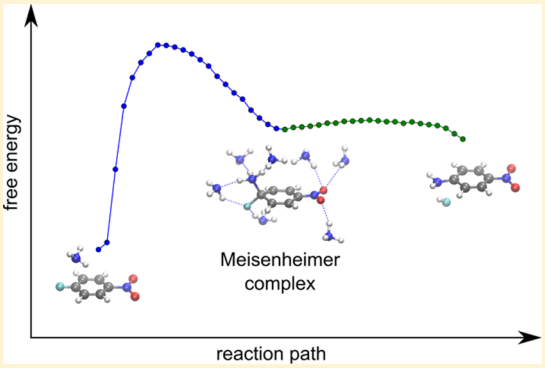

INTRODUCTION

Nucleophilic aromatic substitutions are an essential part of an organic chemist's toolbox.[1−4] These reactions are key steps in the synthesis of various pharmaceutical compounds. Two recent examples are cyclic pyranopterin monophosphate (cPMP) analogues or 3,5-dinitrothiophene scaffolds used in the development of anticancer drugs.[5,6] Knowledge of the mechanism and energetics of nucleophilic aromatic substitution reactions has generated applications beyond their synthetic utility. For example, the susceptibility of electrophilic aromatic compounds to nucleophilic attack has been used to model their skin sensitization potential.[7] The aromatic nucleophilic substitutions of halonitrobenzenes with amines, which are similar to the reactions studied in this article, are of widespread importance, from Sanger's method of peptide sequencing to modern synthetic chemistry and drug design.[8−10]

The most important nucleophilic aromatic substitution mechanisms are the S_NAr, S_N1, benzyne, and $S_{RN}1$ mechanisms.[11] Although these mechanisms have been extensively studied throughout the years, they are still a topic of active research.[12−17] In the case of the S_N1, benzyne, and $S_{RN}1$ mechanisms, the first step is an elimination. Consequently, these reactions require specific substrates and reaction conditions and will not be discussed herein.[18−20] The S_NAr reaction (Scheme 1), which will be central in our study, starts with the attack of a nucleophile on a sufficiently activated, i.e., electron poor, aromatic ring **R**. In the stepwise mechanism, this attack gives rise to a nonaromatic intermediate, called the Meisenheimer complex (**MC**), via transition state $\mathbf{TS_1}$. Subsequent elimination of the leaving group restores aromaticity through a second transition state $\mathbf{TS_2}$, yielding the product **P**. In the concerted mechanism, nucleophilic attack and elimination happen simultaneously, crossing a single barrier through transition state $\mathbf{TS_{conc}}$, and accordingly, no intermediate is formed throughout the process. We note that, while the formal Lewis structures of $\mathbf{TS_{conc}}$ and **MC** as drawn in Scheme 1 are the same, **MC** is a free energy minimum, whereas $\mathbf{TS_{conc}}$ corresponds to an energy maximum along the reaction coordinate.

The first experimental evidence for the stepwise mechanism was given independently by Jackson[21] and Meisenheimer.[22] The intermediate involved in this reaction has since been called a **MC** and has been verified experimentally.[23] The formation of a **MC** via $\mathbf{TS_1}$ is often the rate-determining step in the reaction, although a study on 1-fluoro-2,4-dinitrobenzene illustrated that elimination of fluoride via $\mathbf{TS_2}$ can also be rate determining in specific instances.[24,25] The alternative concerted (one-step) mechanism resembling the S_N2 mechanism has been suggested by Bunnett.[26] On the basis of static gas-phase calculations on

Received: December 10, 2015
Published: January 22, 2016

DOI: 10.1021/acs.joc.5b02794
J. Org. Chem. 2016, 81, 1635−1644

Scheme 1. Concerted and Stepwise Mechanisms for the S_NAr Reaction with NH_3 as the Nucleophile

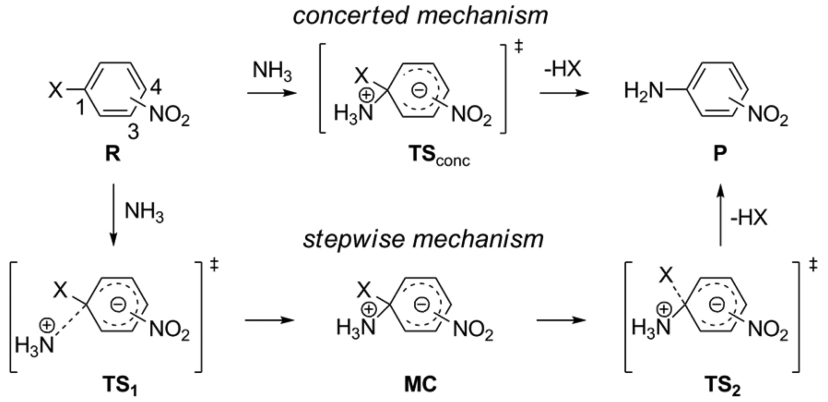

various halobenzenes and halonitrobenzenes, Glukhovtsev et al. suggested a one-step or stepwise mechanism depending on the halide and on the number of activating nitro groups on the ring.[27] It should be mentioned that besides the S_NAr reaction, which typically involves the substitution of a halogen atom, a competing hydrogen substitution may occur through the S_NArH reaction,[28−30] which involves the σ^H addition of a nucleophile at an unsubstituted position, followed by hydrogen elimination through various reaction pathways.

The aim of the present study is to provide a detailed insight into the S_NAr mechanism, choosing liquid ammonia as the solvent with NH_3 as the reacting nucleophile,[29,31] and taking the dynamical factors into explicit account using advanced molecular dynamics simulations. Liquid ammonia shows potential as a green solvent in chemical manufacturing thanks to its low cost and the ease of recycling and product isolation.[32] It has been suggested that liquid ammonia (with a dielectric constant ε = 16.0 at 25 °C) is an advantageous replacement for some dipolar aprotic solvents commonly used for industrial scale aromatic nucleophilic substitution reactions. It is a good H-bond acceptor, with the ability to stabilize ion pairs, it has low surface tension and viscosity, and it is cheaper than most organic dipolar aprotic solvents.[31,33] The rates of S_NAr reactions in liquid ammonia were shown to be similar to those in dipolar aprotic solvents such as DMSO and DMF.[31]

We present a study of the mechanism of S_NAr of several fluoro- and chloro- nitrobenzenes in liquid ammonia for which also experimental rate constants are available. Specifically, we consider the solvolysis reaction of three halonitrobenzenes: 4-nitrofluorobenzene (4-NFB), 2,4-dinitrofluorobenzene (2,4-DNFB), and 4-nitrochlorobenzene (4-NClB) using different theoretical simulation techniques with the aim to fully explore the reaction mechanism and the effect of solvent participation. For these cases, a strong influence of the halogen and the number and position of substituents are noticed as reviewed in several literature works.[28,29,31] First, static density functional theory calculations are performed with various solvation models where the substrate is surrounded by small clusters of solvent molecules. Next, extended ab initio molecular dynamics (AIMD) and metadynamics simulations are performed on the reaction of several halonitrobenzenes with ammonia. Some of these simulations are performed in the gas phase as well as being fully solvated in a liquid ammonia periodic box. For the simulations in liquid ammonia, we introduce a two-stage approach combining metadynamics and committor simulations to obtain a full account of the reaction pathway and assess the stability of the **MC**. In line with previous works,[28,29,31] special attention is given to the role of the solvent in the various stages of the reaction, the influence of the halide, and the number of electron-withdrawing nitro substituents. The resulting trends in reactivity are compared with available experimental kinetic studies. Finally, the possibility of NH_3 addition at the *meta* position relative to the halide, as opposed to the *ipso* addition leading up to the S_NAr reaction, is investigated.

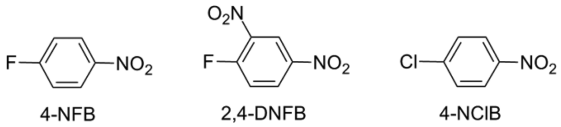

RESULTS AND DISCUSSION

Influence of Solvation on the NH_3 Addition from Static Calculations. Initially, the mechanism of the S_NAr reaction of three nitrohalobenzenes, 4-NFB, 2,4-DNFB, and 4-NClB, with NH_3 is investigated using static cluster calculations. We first consider the addition of one NH_3 molecule at the *ipso* position of the halogen substituent X (X = F or Cl) in the gas phase. The gas-phase calculations indicate high kinetic barriers for the three systems ($\Delta F^{\ddagger}$ > 80 kJ/mol), although the reaction is exergonic for all systems (Figure 1). The ordering of calculated gas-phase activation barriers is 2,4-DNFB < 4-NClB < 4-NFB. Relative to 4-NFB, the introduction of an *o*-nitro group lowers both the Helmholtz free energy barrier $\Delta F^{\ddagger}$ (by 103 kJ/mol) and reaction free energy ΔF_R (by 23 kJ/mol). The chloro substituted analogue is also kinetically more prone to nucleophilic substitution than 4-NFB (by 25.5 kJ/mol), but its free energy of reaction is increased (by 16.3 kJ/mol). Interestingly, as shown in Figure S1, if we follow the intrinsic reaction coordinate (IRC) from the transition state for NH_3 addition toward the product (**P**), an intermediate **MC** is formed for 2,4-DNFB, whereas the aminolysis of both 4-NFB and 4-NClB takes place without such an intermediate, i.e., via an elementary reaction step with a single transition state ($\mathbf{TS_{conc}}$). The geometrical parameters of the $\mathbf{TS_{conc}}$ and **MC** conformations are given in Table S1.

To study the influence of solvation on the mechanism and energetics, NH_3 solvent molecules are gradually added to the system. As is shown in Figure 1, including explicit solvent molecules strongly lowers the barrier of NH_3 addition, as well as the reaction energy. Analysis of the statically determined IRCs shows that, as the number of NH_3 molecules increases, a stable **MC** intermediate appears for the 4-NFB system, similar to the one found with 2,4-DNFB, as mentioned above.

DOI: 10.1021/acs.joc.5b02794
J. Org. Chem. 2016, 81, 1635−1644

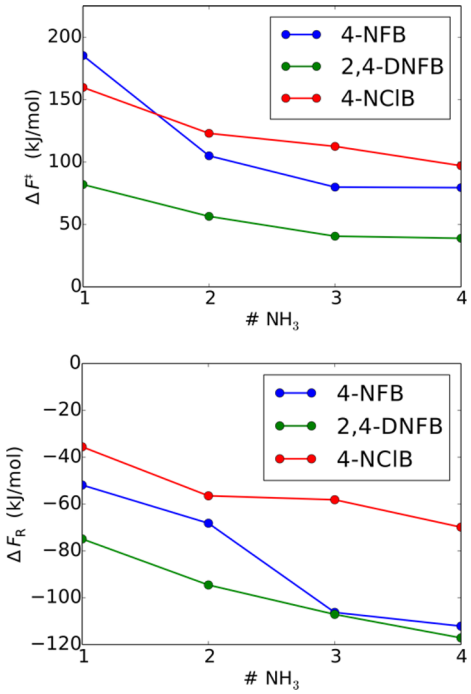

Figure 1. (Top) Free energy barriers of the NH_3 addition step and (bottom) reaction free energies, from static calculations with an increasing number of explicit NH_3 molecules.

Accordingly, the S_NAr reaction with 4-NFB seems to be affected the most by the solvent molecules. It is also clear from Figure 1 that solvation effects are not fully accounted for, as both the barriers heights and the reaction energies are still decreasing when going from three to four explicit NH_3 molecules. Moreover, a proton must be transferred from the reacting NH_3 to the solvent somewhere along the reaction pathway, which severely complicates locating a second transition state ($\mathbf{TS_2}$), if present. This proton transfer indeed greatly facilitates the halide elimination step, as will be shown in the following section. The barriers for the elimination step ($\mathbf{TS_2}$) shown in Figure S1 do not take proton transfer to the solvent into account, and are thus greatly overestimated. At this point, we turn from static cluster calculations to fully periodic AIMD simulations in order to make a definitive conclusion about the reaction mechanism.

Benchmarking the Liquid Ammonia Structure from Ab Initio Molecular Dynamics. As is well-known, similar to water, liquid ammonia is a protic solvent that forms hydrogen bonds between NH_3 molecules. As will be shown below, H-bond interactions with ammonia are an essential part of the S_NAr reaction mechanism. Radial distribution functions (RDFs) provide an insight into the characteristic intra- and intermolecular interactions of the solvent. The positions and widths of the peaks in the RDF reflect favored atom−atom distances and their variations. The RDFs are thus well suited to compare the degree of H-bond formation and H-bond distances of the simulated liquid ammonia with those of experiment and other computational studies.

In Figure 2, the RDFs, g_{H-H}, g_{N-H}, and g_{N-N}, are shown for liquid ammonia at 273 K, obtained from a 30 ps equilibration, followed by a 40 ps production MD run. The RDFs are very similar to the ones calculated from Car−Parrinello MD simulations by Diraison and Martyna[34] and reproduce very well the partial RDF data from neutron diffraction measure-

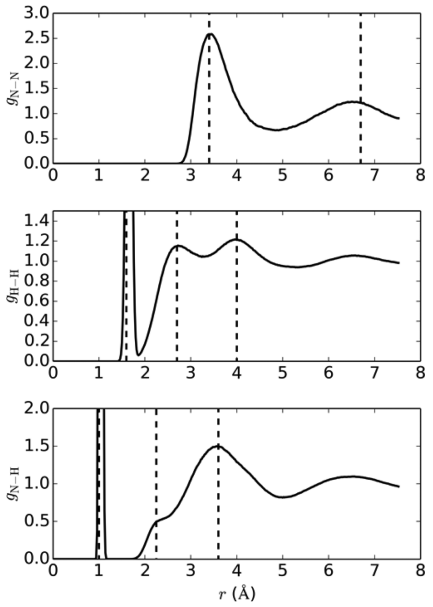

Figure 2. RDFs of liquid ammonia from a 70 ps AIMD simulation at 273 K: (top) g_{N-N}, (middle) g_{H-H}, and (bottom) g_{N-H}. Dashed lines indicate the positions of the experimental peaks.

ments of Ricci et al.[35] at 273 K. The positions of both the intramolecular and intermolecular peaks coincide very well with those obtained from experiment. The experimentally determined intramolecular peaks are broader, an effect that is attributed to quantum dispersion.[34] Quantum dispersion, arising from quantum nuclear dynamics, is not captured by the AIMD method, which provides a classical treatment of the nuclei dynamics. The two broad peaks in g_{N-N} represent the first and second solvation shells (Figure 2, top). As calculated from the RDF, on average 12.7 neighboring N atoms are within the (experimentally determined) first solvation shell at a r_{N-N} = 5.2 Å, close to the experimental value,[35] which is on the order of 14. Similarly, 42.0 H atoms are found within the first solvation shell at r_{H-H} = 5.2 Å, matching the experimental value, on the order of 42. The small shoulder in g_{N-H} at 2.2 Å (Figure 2, bottom), characteristic of H-bonding, is well reproduced in the simulation, while the broad peak at 3.6 Å, corresponding to nonspecific interaction between NH_3 molecules in the first solvation shell, is slightly overestimated.

Overall, the excellent agreement of intermolecular structure with experimental data demonstrates that the simulation method employed in this study is appropriate for the liquid ammonia solvent.

Substitution of 4-Fluoronitrobenzene in Gas Phase with Metadynamics. Initially, a reference metadynamics simulation is performed in the gas phase at 298 K. The S_NAr reaction of 4-NFB with one NH_3 is chosen as the reference system. Although NH_3 addition can occur at different positions on the benzene ring, only addition at the *ipso* position relative to the halide may result in a S_NAr substitution reaction (the alternative *meta* addition is also investigated; see below). Simulating the substitution reaction in the gas phase is relatively straightforward because only one NH_3 molecule is available for addition to the benzene ring, and once the 4-amino-nitrobenzene (4-ANB) product is formed, only one proton is available to recombine with the NH_2 group in the reverse reaction. The metadynamics simulation is carried out with two collective variables. The C−F and C−N bonds are activated

DOI: 10.1021/acs.joc.5b02794
J. Org. Chem. 2016, 81, 1635−1644

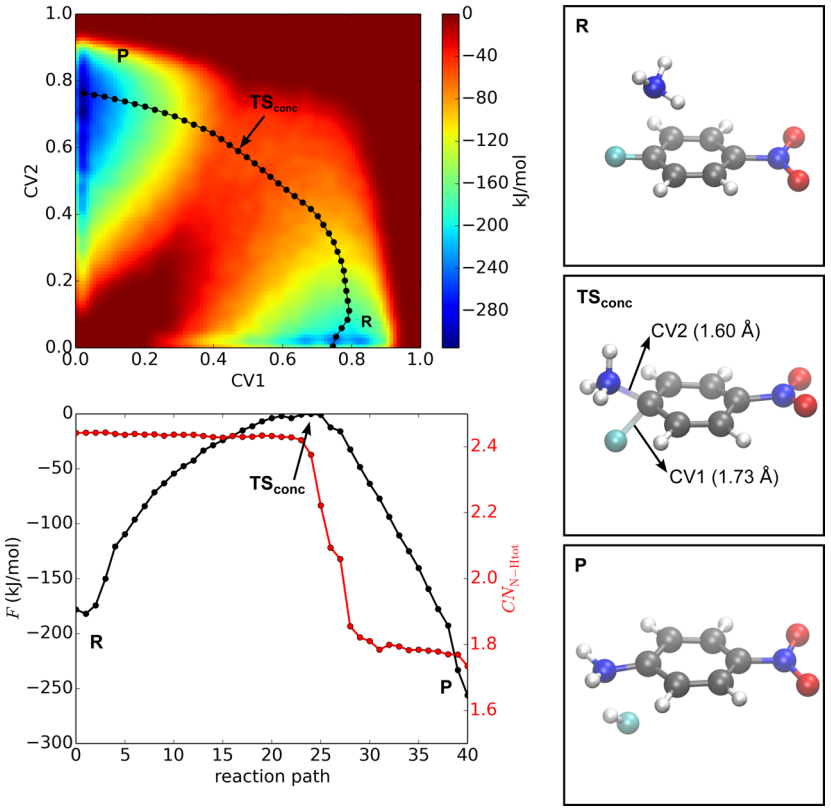

Figure 3. (top left) 2D free energy surface for the gas-phase S_NAr reaction of 4-NFB with one NH_3. The 1D reaction pathway (black circles) is obtained from a NEB calculation. (bottom left) PMF (black) and average $CN_{N\text{-}Htot}$ (red), indicating proton transfer from NH_3 to F^-, along the 1D path. (right) Representative snapshots of the **R**, **TS$_{conc}$**, and **P** states.

simultaneously by placing 2-dimensional (2D) Gaussian hills along two collective variables (CVs): coordination numbers CN_{C-F} (CV1) and CN_{C-N} (CV2). No bias has to be introduced to directly stimulate the proton transfer because this event is essentially barrierless and occurs very frequently during the simulation. The resulting free energy surface is shown in Figure 3. Initial and final states **R** and **P** correspond to CV1 and CV2 values ~0.8, respectively, which follows from the definition of *CN* (see Computational Methods section). Clearly, no intermediate state is formed, confirming the results of the gas phase static calculations. A nudged elastic band (NEB) calculation on the 2D free energy surface results in a 1-dimensional (1D) free energy profile or potential of mean force (PMF) (Figure 3). Following the PMF from reactant to product, a relatively flat plateau region precedes **TS$_{conc}$** (steps 20–24). In this region, both ammonia and fluorine are bound to the C_1 atom. The transition state is reached rather late, the C–F bond being partially broken (r_{C-F} = 1.80 Å) and the C–N bond almost fully formed (r_{C-N} = 1.60 Å), similar to the static calculations (Table S1). After **TS$_{conc}$**, a steep downhill pathway is followed toward the product state. Importantly, the onset of the downhill curve coincides with a proton transfer from NH_3 to the fluoride anion, as is evidenced by the sudden drop in the total N–H coordination ($CN_{N\text{-}Htot}$) at **TS$_{conc}$** (Figure 3). This unambiguously shows that the fluoride elimination is assisted by proton transfer.

Substitution of 4-Fluoronitrobenzene in Liquid Ammonia: A Two-Stage Approach. AIMD simulations are now performed in a liquid ammonia periodic box, taking into full account the dynamic nature of the solvent electric field, its hydrogen bonding capacity, and its proton affinity. In moving to the liquid ammonia environment, however, it is not possible to fully adopt the metadynamics strategy that was used in the gas phase. While in the gas phase the released proton combines with the eliminated F^- to form HF, this is often not the case in the solvent. Rather, the proton is quickly transferred to a nearby NH_3 molecule and then to bulk ammonia. It is clear that at this point on the reaction path, the probability that the system returns to the reactant state is vanishingly small. We have therefore adopted a two-stage strategy. In the first (metadynamics) stage, we concentrate on the NH_3 addition step. The same metadynamics parameters are used as introduced for the gas phase simulations but with additional potential walls to keep the three H atoms of the reacting NH_3 bound to the N atom, thus allowing the system to easily go back to the reactant state. Application of the potential walls is justified by the observation that the N atom of the reacting NH_3 remains coordinated with three H atoms during the NH_3 addition step. We have verified that this is indeed the case during several forward reaction events observed in independent metadynamics simulations without additional potential walls, and in a 20 ps MD simulation that is restrained at **TS$_1$**. For the second step, the halide elimination, the committor analysis is performed with 200 independent AIMD simulations with starting coordinates located at **TS$_1$**. The committor simulations serve three functions. First, they provide additional evidence of the exact location the transition state, provided that about half of the simulations end up in the product state. Second, from the simulations that reach the product state, the stability of the **MC** intermediate and the rate of product formation starting from the **MC** can be calculated. Because proton transfer to the solvent is very fast, only a few ps are needed to reach the

DOI: 10.1021/acs.joc.5b02794
J. Org. Chem. 2016, 81, 1635–1644

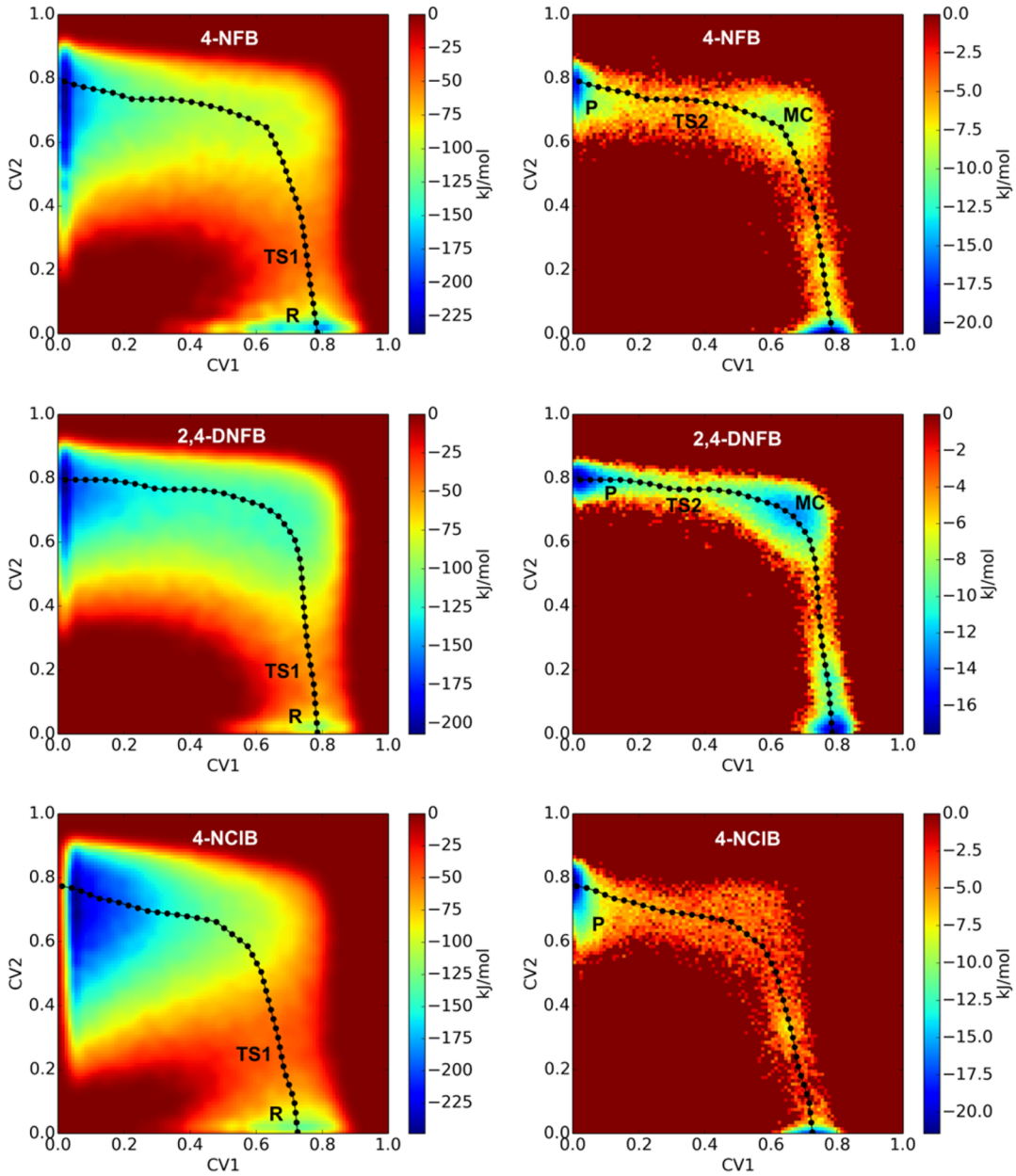

Figure 4. 2D free energy surfaces for the S_NAr reaction of (top) 4-NFB, (middle) 2,4-DNFB, and (bottom) 4-NClB with NH_3 in liquid ammonia. (Left) Restrained metadyanamics simulations. (Right) Committor analysis. The 1D reaction pathways (black circles) are obtained from NEB calculations on the committor surfaces.

product state. Thus, crossing $\mathbf{TS_2}$ from **MC** does not require enhanced sampling techniques such as metadynamics. Third and most importantly, these committor simulations can be combined and analyzed to gain insight into the mechanism and the role of the solvent.

The free energy barrier for the addition of NH_3, as obtained from the metadynamics stage, is much lower in liquid ammonia than in gas phase, as predicted by extrapolating the static calculations with increasing number of explicit solvent molecules (Figure 4 and Table 1). Relative to $\mathbf{TS_{conc}}$ in the gas-phase reaction, the position of $\mathbf{TS_1}$ on the 2D free energy surface has moved toward the reactant state. At $\mathbf{TS_1}$, the C−N bond is only partly formed (r_{C-N} = 2.05 Å), while the C−F bond is still intact (r_{C-F} = 1.41 Å) (Figure 4).

Of the 200 committor simulations, 107 ended up in the product state, confirming $\mathbf{TS_1}$ as determined in the metadynamics stage. After combining all of the committor data, an approximate 2D free energy surface is constructed (Figure 4), revealing a stable Meisenheimer intermediate. The stability of the **MC** state is, however, very low. The **MC**-to-**P** rate is calculated by plotting the number of transition events from $\mathbf{TS_1}$ to $\mathbf{TS_2}$ as a function of time (Figure S1). This curve is fitted with a kinetic equation comprising a lag phase followed by two consecutive first-order reactions (eq 1 in Computational Methods section). The lag phase represents the initial time spent on top of $\mathbf{TS_1}$; the first first-order reaction corresponds to the downhill motion from $\mathbf{TS_1}$ to **MC**; the second first-order reaction gives an estimate of the actual **MC**-to-**P** rate. The calculated rate constant for the second step k_2 = 4.3 ps^{-1}, with

DOI: 10.1021/acs.joc.5b02794
J. Org. Chem. 2016, 81, 1635−1644

Table 1. Free Energy Barriers and Rate Constants in Liquid Ammonia and Comparison with Experiment[a]

	AIMD					Static		
	step 1 (metadynamics)			step 2 (committor)		step 1		meta
substrate	$\Delta F^{\ddagger}_1$	k_1	k_{exp}	$\Delta F^{\ddagger}_2$	k_2	$\Delta F^{\ddagger}_1$	k_1	$\Delta F^{\ddagger}_{meta}$
4-NFB	108	7.3×10^{-7}	7.86×10^{-6}	0.9	4.3×10^{9}	79	8.8×10^{-2}	75
2,4-DNFB	41	4.0×10^{5}	$>1.40 \times 10^{-1}$	2.1	2.6×10^{9}	39	9.1×10^{5}	52
4-NClB	81	3.9×10^{-2}	no reaction			97	6.2×10^{-5}	79

[a]Helmholtz free energy values ($\Delta F^{\ddagger}$) are in kJ/mol and rate constants (k) in (s^{-1}). The k_1 values are calculated from $\Delta F^{\ddagger}_1$ using standard transition state theory: $k = k_B T/h \exp(-\Delta F^{\ddagger}/k_B T)$. Likewise, the $\Delta F^{\ddagger}_2$ values are calculated from k_2 using the same formula. Static calculations are performed in the presence of four explicit NH_3 solvent molecules. The designation "meta" refers to σ^{H} addition *meta* to the halogen.

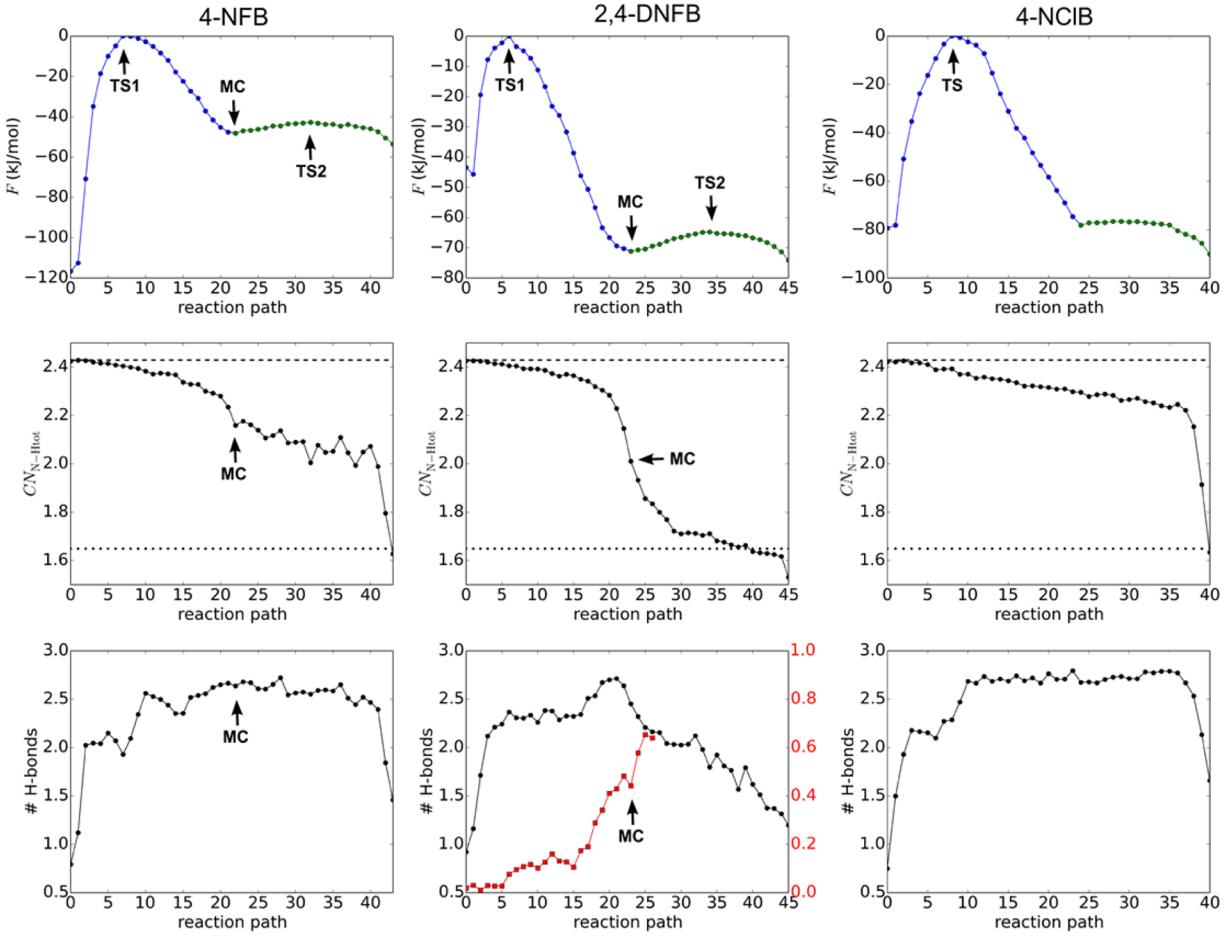

Figure 5. (Top row) Approximate global 1D PMF of the S_NAr reaction with NH_3 in liquid ammonia, obtained from metadynamics (blue) and committor (green) simulations. (Middle row) $CN_{N\text{-}Htot}$ of the reacting NH_3 along the reaction path. The dashed and dotted lines indicate a three- and two-coordinated N atom in the optimized product state, respectively. (Bottom row) Average number of donating H-bonds from the reacting NH_3 to the liquid ammonia solvent along the reaction path. (Left column) 4-NFB, (middle column) 2,4-DNFB, and (right column) 4-NClB. Red squares and right axis indicate the H-bond probability between the reacting (protonated: $CN_{N\text{-}Htot} > 2.35$) NH_3 and the *o*-nitro group of 2,4-DNFB.

the corresponding free energy barrier $\Delta F^{\ddagger}_2$ = 0.9 kJ/mol. This computed barrier height may be somewhat underestimated because the system spends just a short amount of time in the **MC** state, which may not be enough to dissipate its excess kinetic energy to the surroundings. The 1D PMFs of the metadynamics and committor simulations can be combined to obtain an approximate global 1D PMF of the S_NAr reaction, as shown in Figure 5 (top row).

Representative snapshots of $\mathbf{TS_1}$, **MC**, and $\mathbf{TS_2}$ are shown in Figure 6. As can be seen, many stabilizing H-bond interactions with solvent molecules are present during all phases of the reaction. Liquid ammonia forms up to four donating H-bonds with the nitro group, whereas up to two donating H-bonds are formed with the leaving fluoride. Three ammonia molecules form accepting H-bonds with the reacting NH_3, until its proton is transferred to the solvent (Figure 5, middle and bottom rows). The protonation state of **MC** (Figure 5, middle row) is predominantly zwitterionic for 4-NFB, whereas for 2,4-DNFB **MC** is about 50% zwitterionic and 50% anionic. Collectively, these dynamic but specific interactions form the dominant contributing factor in the solvent stabilization of transition states and **MC**.

Role of the Solvent. We now combine all of the data of the committor simulations to follow the degree of hydrogen bond

DOI: 10.1021/acs.joc.5b02794
J. Org. Chem. 2016, 81, 1635−1644

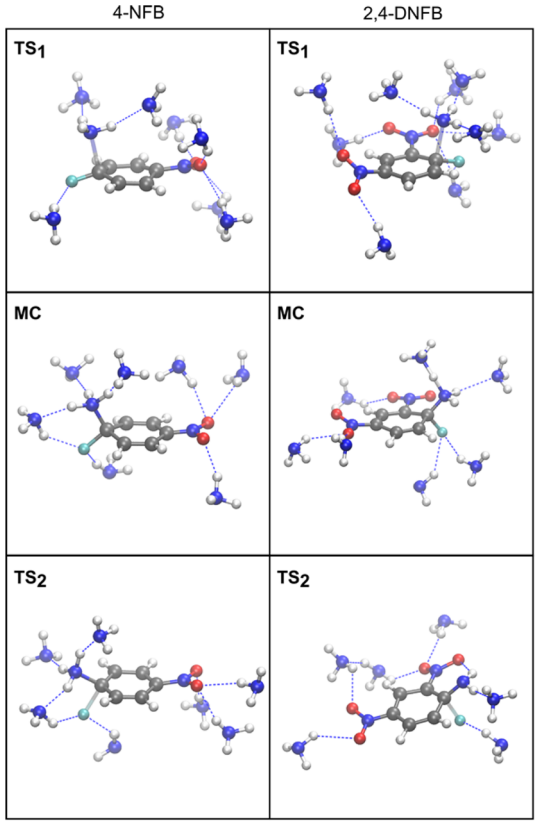

Figure 6. Representative snapshots of $\mathbf{TS_1}$, **MC**, and $\mathbf{TS_2}$ for 4-NFB (left) and 2,4-DNFB (right). Hydrogen bonds are indicated with blue dashed lines.

formation during the reaction (Figure 5, bottom row). In the reactant state, while in principle the reacting NH_3 may donate three H-bonds with neighboring solvent molecules, on average about one donating H-bond is present between the reacting NH_3 and the solvent. The degree of hydrogen bonding quickly increases to about 2.5 at $\mathbf{TS_1}$ and stays constant until the reaction gets beyond $\mathbf{TS_2}$, after which it quickly drops to 1.5 in the product state. It is clear that such a high degree of hydrogen bonding has a strong stabilizing effect on both transition states. We also follow the protonation state of the reacting NH_3, calculated as the total number of H atoms coordinated with the N atom (Figure 5). The N atom remains coordinated with three H atoms until after $\mathbf{TS_1}$, where the curve gradually decreases to $CN_{\text{N-Htot}} \cong 2.1$ until well past $\mathbf{TS_2}$, after which the proton is quickly removed in the product state. Thus, the role of the solvent is 2-fold. In the addition step, it drastically lowers the barrier and stabilizes the **MC** by extensive H-bond formation of the reacting NH_3 with 2.5 NH_3 molecules on average. In the elimination step, elimination of F^- is greatly facilitated by proton transfer from the reacting NH_3 to the solvent. The rates of S_NAr in liquid ammonia are comparable with those in DMSO,[31] despite its much lower dielectric constant (16.0 versus 46.7). Our results clearly show that the ability of liquid ammonia to act as a strong H-bond acceptor makes up for its reduced polarity.

Influence of Substituents. The same strategy as described above is used to study the aromatic substitution of the two 4-NFB analogues. In 2,4-DNFB, the extra electron withdrawing *o*-nitro group further lowers the free energy of $\mathbf{TS_1}$ and **MC** relative to the reactant state (Figure 5). Additional stabilization is provided by an intramolecular H-bond between the reacting (protonated) NH_3 and the *o*-nitro group (Figure 5, red squares), also known in the literature as the "built-in solvation" effect.[36−38] The **MC** state is, however, only slightly stabilized kinetically, as $\mathbf{TS_2}$ is also lowered in energy. The origin of the lowered $\mathbf{TS_2}$ is found in the degree of deprotonation of the reacting NH_3. Whereas about half of the 4-NFB structures are protonated at $\mathbf{TS_2}$, almost all 2,4-DNFB structures are deprotonated at $\mathbf{TS_2}$ (Figure 5). The increased deprotonation rate can be rationalized by the electron withdrawing effect of the *o*-nitro group, as well as by an intramolecular H-bond between the (deprotonated) NH_2 group and the *o*-nitro group (see Figure 6).

With the chloro analogue (4-NClB), the reaction follows a single-step mechanism in solvent (Figure 5). After the addition product is formed, the PMF remains essentially flat until very late along the 1D reaction pathway, where it suddenly drops. The $CN_{\text{N-Htot}}$ value also remains very high until right after the free energy drop toward the product (Figure 5). Taken together, these data suggest that elimination of Cl^- is essentially barrierless and relatively independent of the protonation state of the reacting NH_3.

In Table 1, the results are summarized and compared with the static calculations and with experimental pseudo-first-order rate constants (k_{exp}).[31] Although aiming to accurately reproduce activation barriers is beyond the scope of this study, the calculated $\Delta F^{\ddagger}_1$ and k_1 trends for 4-NFB and 2,4-DNFB are in agreement with rate constants from the experiment.

Deactivating σ^H Addition of NH_3. Remarkably, no reaction was observed experimentally with 4-NClB, even though the free energy barrier obtained from metadynamics is lower than that of 4-NFB. A likely explanation for this apparent contradiction is provided by a competing deactivating reaction, in particular the σ^H addition of NH_3 at an unsubstituted position *meta* to the halogen substituent and *ortho* to a nitro group (Scheme 2).[31] Experimentally, the high

Scheme 2. σ^H Addition of NH_3 onto Nitrohalobenzenes

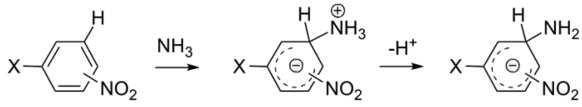

reactivity of nitroarenes toward nucleophilic addition in *ortho* to a nitro group is well-known, and is in fact taken advantage of in various nucleophilic aromatic hydrogen substitution (S_NArH) reactions. According to the static calculations (Table 1), the *meta*-halogen addition reaction is competitive with addition at the *ipso* position, at least for 4-NFB and 4-NClB. With 4-NClB as the substrate, the barrier difference of *meta* versus *ipso* addition $\Delta F^{\ddagger}_{\text{meta}} - \Delta F^{\ddagger}_1 = -18$ kJ/mol, while for 4-NFB, the difference between the two barriers is only 4 kJ/mol. These results are consistent with the reduced mesomeric electron donating effect of chlorine versus fluorine, despite fluorine having a higher inductive electron-withdrawing effect. Indeed, fluorobenzene is more reactive toward electrophilic aromatic substitution than chlorobenzene. These results are supported by experimental data, showing that substitution at the fluoro position is competitive with σ^H addition *ortho* to a nitro group, while substitution at the chloro position is much slower.[39−41]

To further investigate the possibility of σ^H addition, three independent MD simulations are performed starting from the

DOI: 10.1021/acs.joc.5b02794
J. Org. Chem. 2016, 81, 1635−1644

meta-ammonium adduct of 4-NClB. In all three cases, a proton is quickly transferred from the reacting NH_3 to a nearby NH_3 molecule after 1−9 ps. In this hydrogen bonded state, the NH_4^+ ion is ready to donate its proton back and allow the reverse elimination reaction to occur. However, the NH_4^+ ion is not strongly H-bonded with the *meta*-amino adduct, as it diffuses into the bulk solvent after 1−5 ps. This behavior suggests that the ammonium ion prefers to be in the bulk solvent environment, rather than being hydrogen bonded to the *meta*-amino adduct. Thus, in the case of 4-NClB, the σ^H addition pathway leads to a complete deactivation of the S_NAr reaction by formation of a stable 3-amino,4-nitrochlorobenzene anion (Scheme 2). Note that, given the nature of the nucleophile and the reaction conditions (no protic media, strong bases, or oxidants), further reaction of the σ^H adduct in liquid ammonia is unlikely.

CONCLUSIONS

A thorough mechanistic study of the solvolysis of selected halonitrobenzenes in liquid ammonia is presented. The reactivity of 4-NFB, 2,4-DNFB, and 4-NClB toward S_NAr substitution with NH_3 was investigated in the gas phase as well as in liquid ammonia. Initial static cluster calculations revealed that the S_NAr reaction is strongly affected by hydrogen bonding interactions with the solvent. Whereas the first (NH_3 addition) step could be usefully modeled with a static approach, in the second (halide elimination) step static approaches are unable to reliably take into account proton rearrangement from the reacting NH_3 to the solvent.

To fully account for solvent effects, AIMD simulations in a periodic solvent box were performed. The accuracy of the simulations was assessed by benchmarking the RDFs of liquid ammonia against neutron diffraction measurements, showing excellent agreement with experiment. The complexity of the S_NAr reaction was reduced by adopting a two-stage approach. In the first stage, we performed two-dimensional metadynamics simulations to calculate the free energy barrier of NH_3 addition step and to locate the first transition state. In the second stage, committor simulations were performed to evaluate the stability of the intermediate **MC** and the rate of product formation. The simulation data predict a two-step mechanism for 4-NFB and 2,4-DNFB, whereas the reaction with 4-NClB proceeds via a concerted one-step mechanism. Analysis of the committor simulations revealed that the reaction is highly dependent on dynamic interactions between the reacting NH_3 and the solvent, most notably hydrogen bonding and proton transfer to the bulk solvent.

The calculated rate constants for 4-NFB and 2,4-DNFB are consistent with experimental pseudo-first-order rate constants. For 4-NClB, however, no reaction was observed despite the relatively high calculated rate constant. Additional static calculations and AIMD simulations elucidated a likely explanation for the inability of 4-NClB to undergo S_NAr substitution through the occurrence of a deactivating, experimentally well-known σ^H addition pathway.

In summary, we have shown that the two-stage approach employed in this work, involving a combination of metadynamics-commitor simulations in gas phase as well as on a fully solvated system, allowed one to identify a shift from a one-step concerted mechanism in gas phase to a two-step mechanism in liquid ammonia. To verify whether the obtained mechanistic insights can be generalized to the S_NAr reaction, we are currently investigating a larger data set with more diverse aromatic compounds and different nucleophiles.

COMPUTATIONAL METHODS

Static Calculations. All static calculations are carried out using density functional theory (DFT) according to the Kohn−Sham scheme as implemented in the Gaussian 09 program package.[42] Geometry optimizations are performed with the M06-2X exchange-correlation functional[43] and the 6-31+G(d,p) basis set.[44] Analytical vibrational frequencies are computed within the harmonic approximation to confirm convergence to well-defined minima or saddle points on the potential energy surface. All transition states are verified by following the reaction path by an integration of the intrinsic reaction coordinate (IRC).[45−47] A key point is the fact that ammonia serves both as solvent and as nucleophile in the S_NAr reaction studied here. Accounting for the solvation environment in these reactions thus has to go beyond implicit solvation. The most straightforward is the supermolecule or cluster approach in which explicit ammonia molecules are added to the system. Because of the possibility of specific intermolecular interactions such as H-bonds, explicit solvation is often required to obtain accurate results.[48−53] In this work, up to three solvating ammonia molecules are added to the reaction systems. It has to be mentioned that this approach logically tends to be more difficult and tedious with increasing amounts of explicit solvent molecules added.

Molecular Dynamics. The AIMD simulations are performed with the CP2K simulation package (version 2.6).[54] At each MD step, the self-consistent field energies are calculated at the DFT level with the gradient-corrected BLYP functional,[55,56] the DZVP−GTH basis set,[57] and Grimme D3 dispersion corrections.[58] AIMD simulations with the BLYP functional have been shown to reproduce well the local structure of liquid ammonia,[34] and of water,[59] the latter in combination with dispersion corrections. Additionally, barriers for SN_2 and E_2 reactions calculated with the BLYP functional were in good agreement with high-level (MP2) calculations.[60] Basis set superposition error and nuclear quantum effects are not taken into account.[61,62] The integration time step is set at 1 fs. Simulations in liquid ammonia are performed in the NVT ensemble, using the "canonical sampling through velocity rescaling" thermostat[63] with a time constant of 50 fs. The reactant is placed inside a periodic cubic box filled with 80 NH_3 molecules. The density of liquid ammonia is set to the experimental density at 273 K (0.639 g/mL). For pure ammonia, solvated 4-NFB, 2,4-DNFB, and 4-NClB, the corresponding box lengths are 15.240, 15.382, 15.547, and 15.571 Å, respectively. To match the experimental temperatures, simulations of pure liquid ammonia are performed at 273 K, while aromatic substitution reactions are performed at 298 K. The pure ammonia simulation was continued for 70 ps until convergence as defined by the height of the first peak in the g_{N-N} RDF (Figure 2), which differed by <0.05 between the last two 20 ps parts of the simulation.

Metadynamics. To explore chemical reactions using molecular dynamics simulations, advanced techniques need to be used to sample the low probability regions of the potential energy surface.[64−66] Herein we use the metadynamics technique introduced by Laio and Parrinello,[67,68] which relies on the choice of a limited number of collected variables along which the sampling is enhanced by adding Gaussian hills along these coordinates, and has been successfully used in a variety of systems.[69−71]

The metadynamics simulations are performed by placing Gaussian potential hills every 25 steps along two collective variables (CVs). The CVs used in this work are coordination numbers, defined as $CN_{i-j} = [1 - (r_{i-j}/r_0)^6]/[1 - (r_{i-j}/r_0)^{12}]$, where r_{ij} is the distance between atoms i and j, and r_0 is a reference distance. The first CV, $CN_{C\text{-}X}$, follows the bond breaking between C_1 and the halogen atom, with r_0 = 1.7 and 2.1 Å for C_1−F and C_1−Cl, respectively (for numbering of C atoms, see Scheme 1). The second CV, CN_{C-N}, is given by the C−N bond between C_1 and the reacting NH_3, with r_0 = 1.7. All r_0 values were chosen to be close to the transition state distances, as determined from static calculations. The width of the Gaussian hills is set to 0.02, and

DOI: 10.1021/acs.joc.5b02794
J. Org. Chem. 2016, 81, 1635−1644

their height is initially set to 5 kJ/mol. After reaching the product state and returning to the reactant state for the first and second time, the height is reduced to 2.5 and 1.25 kJ/mol, respectively. The reacting NH_3 and the leaving halide are kept close to the reaction center by applying attractive walls at CN = 0.015 to both CV1 and CV2, with a force constant of 200 hartree. In the metadynamics simulations in liquid ammonia, additional distance restraints are applied to the three N−H distances at r_{N-H} = 1.04 Å, corresponding to the equilibrium N−H distance, with a force constant of 100 kJ/mol Å^2. The metadynamics simulations had to be continued until the combined Gaussian hills amounted to 60 kJ/mol at the transition state to obtain converged free energy barriers, corresponding to simulation times of 230−340 ps. On the basis of the resulting 2D free energy surface, a 1D reaction pathway is computed with a NEB calculation.[72]

Committor Analysis. The concept of committor distributions was introduced by Bolhuis et al.[73] for analyzing reaction coordinates and locating free energy barriers. For each solvated system, a large number of committor simulations with starting coordinates located at $\mathbf{TS_1}$ are performed. The (200) starting coordinates and velocities are the snapshots taken every 100 fs from a 20 ps MD simulation restrained at $\mathbf{TS_1}$. Each simulation is continued without any restraints until the reactant (**R**) or product (**P**) state is reached; in the latter case, the reaction proceeds via **MC**. The reaction events obtained from the committor simulations that end up in **P** are used to obtain the rate for the **MC**-to-**P** reaction step. The data are fitted to a kinetic equation (eq 1) consisting of a lag time followed by two consecutive first order reactions:

$$[\mathrm{P}](t) = [\mathrm{TS_1}]_0\left(1 + \frac{k_a e^{-k_2(t-t_{lag})} - k_2 e^{-k_a(t-t_{lag})}}{k_2 - k_a}\right) \quad (1)$$

where [**P**] is the product concentration, $[\mathbf{TS_1}]_0$ is the initial $\mathbf{TS_1}$ concentration, k_a is the rate constant for the $\mathbf{TS_1}$-to-**MC** transition, and k_2 is the rate constant for the **MC**-to-**P** reaction. The product is formed once $\mathbf{TS_2}$ has been crossed. According to the kinetic curves (Figure S2), a minimum amount of time (∼40 fs) is needed for the system to cross $\mathbf{TS_2}$. The lag time t_{lag} thus corresponds to time needed to travel the reaction coordinate from $\mathbf{TS_1}$ to $\mathbf{TS_2}$ in the case of an immediate reaction event. In the structural analysis of the committor simulations, H-bonds are computed as the sum of the donor-H and H-acceptor distances with a cutoff distance of 3.5 Å. The total N−H coordination of the reacting NH_3 ($CN_{N\text{-}Htot}$) is calculated as the sum of the three CN_{N-H} values, with r_0 = 1.325 Å.

■ ASSOCIATED CONTENT

Supporting Information

The Supporting Information is available free of charge on the ACS Publications website at DOI: 10.1021/acs.joc.5b02794.

Free energy profiles from static calculations; geometrical parameters and charges of $\mathbf{TS_{conc}}$ and **MC** from static calculations; kinetic curves of the $\mathbf{TS_1}$-to-$\mathbf{TS_2}$ transiton (PDF)

Cartesian coordinates of $\mathbf{TS_1}$/$\mathbf{TS_{conc}}$ from static calculations and absolute free energies (PDF)

■ AUTHOR INFORMATION

Corresponding Author

*E-mail: samuel.moors@vub.ac.be.

Notes

The authors declare no competing financial interest.

■ ACKNOWLEDGMENTS

The computational resources and services used in this work were provided by the VSC (Flemish Supercomputer Center), funded by the Hercules Foundation and the Flemish Government, department EWI. P.G. and F.D.P. thank the Fund for Scientific Research - Flanders (FWO) and the Vrije Universiteit Brussel (VUB) for their continuous support. They also specifically mention the Strategic Research Program awarded to the ALGC group by the VUB which started on January 1, 2013. B.P. thanks the FWO for awarding a postdoctoral fellowship (12794414N). D.H., S.C., and V.V.S. acknowledge the FWO, the Research Board of Ghent University (BOF), and BELSPO in the frame of IAP/7/05 for support.

■ REFERENCES

(1) Clark, G. R.; Ferguson, L. A.; McIntosh, A. E.; Söhnel, T.; Wright, L. J. *J. Am. Chem. Soc.* **2010**, *132*, 13443.
(2) Tsuchimoto, T.; Iwabuchi, M.; Nagase, Y.; Oki, K.; Takahashi, H. *Angew. Chem., Int. Ed.* **2011**, *50*, 1375.
(3) Woydziak, Z. R.; Fu, L. Q.; Peterson, B. R. *J. Org. Chem.* **2012**, *77*, 473.
(4) Terrier, F. *Modern Nucleophilic Aromatic Substitution*; Wiley-VCH: Weinheim, 2013.
(5) Hilken, S.; Kaletta, F.; Heinsch, A.; Neudörfl, J.-M.; Berkessel, A. *Eur. J. Org. Chem.* **2014**, *2014*, 2231.
(6) Sarkar, P.; Maiti, S.; Ghosh, K.; Sengupta, S.; Butcher, R. J.; Mukhopadhyay, C. *Tetrahedron Lett.* **2014**, *55*, 996.
(7) Roberts, D. W.; Aptula, A. O.; Patlewicz, G. Y. *Chem. Res. Toxicol.* **2011**, *24*, 1003.
(8) Sanger, F. *Biochem. J.* **1949**, *45*, 563.
(9) Reddy, M. V.; Akula, B.; Cosenza, S. C.; Athuluridivakar, S.; Mallireddigari, M. R.; Pallela, V. R.; Billa, V. K.; Subbaiah, D. R.; Bharathi, E. V.; Vasquez-Del Carpio, R.; Padgaonkar, A.; Baker, S. J.; Reddy, E. P. *J. Med. Chem.* **2014**, *57*, 578.
(10) Narawane, S.; Budnjo, A.; Grauffel, C.; Haug, B. E.; Reuter, N. *J. Med. Chem.* **2014**, *57*, 1111.
(11) Smith, M. B. *March's Advanced Organic Chemistry: Reactions, Mechanisms, and Structure*; John Wiley & Sons: New York, 2013.
(12) Fernandez, I.; Frenking, G.; Uggerud, E. *J. Org. Chem.* **2010**, *75*, 2971.
(13) Lin, R.; Zhang, H.; Li, S. H.; Wang, J. I.; Xia, H. P. *Chem. - Eur. J.* **2011**, *17*, 4223.
(14) Sperotto, E.; van Klink, G. P. M.; van Koten, G.; de Vries, J. G. *Dalton T* **2010**, *39*, 10338.
(15) Jones, S. G.; Yau, H. M.; Davies, E.; Hook, J. M.; Youngs, T. G. A.; Harper, J. B.; Croft, A. K. *Phys. Chem. Chem. Phys.* **2010**, *12*, 1873.
(16) Acevedo, O.; Jorgensen, W. L. *Org. Lett.* **2004**, *6*, 2881.
(17) Sadowsky, D.; McNeill, K.; Cramer, C. J. *Environ. Sci. Technol.* **2014**, *48*, 10904.
(18) Truong, T.; Daugulis, O. *J. Am. Chem. Soc.* **2011**, *133*, 4243.
(19) Bardagi, J. I.; Rossi, R. A. *J. Org. Chem.* **2010**, *75*, 5271.
(20) Shirakawa, E.; Hayashi, Y.; Itoh, K.; Watabe, R.; Uchiyama, N.; Konagaya, W.; Masui, S.; Hayashi, T. *Angew. Chem., Int. Ed.* **2012**, *51*, 218.
(21) Jackson; Gazzollo. *Am. Chem. J.* **1900**, *23*, 376.
(22) Meisenheimer, J. *Justus Liebigs Annalen Der Chemie* **1902**, *323*, 205.
(23) Chiavarino, B.; Crestoni, M. E.; Fornarini, S.; Lanucara, F.; Lemaire, J.; Maitre, P. *Angew. Chem., Int. Ed.* **2007**, *46*, 1995.
(24) Kavalek, J.; Kubias, J.; Štěrba, V. *Collect. Czech. Chem. Commun.* **1972**, *37*, 4041.
(25) Emokpae, T. A.; Isanbor, C. *Int. J. Chem. Kinet.* **2004**, *36*, 188.
(26) Bunnett, J. F. *Tetrahedron* **1993**, *49*, 4477.
(27) Glukhovtsev, M. N.; Bach, R. D.; Laiter, S. *J. Org. Chem.* **1997**, *62*, 4036.
(28) Makosza, M. *Chem. Soc. Rev.* **2010**, *39*, 2855.
(29) Mąkosza, M. *Chem. - Eur. J.* **2014**, *20*, 5536.
(30) Gulevskaya, A. V.; Tyaglivaya, I. N. *Russ. Chem. Bull.* **2012**, *61*, 1321.
(31) Ji, P.; Atherton, J. H.; Page, M. I. *J. Org. Chem.* **2011**, *76*, 3286.
(32) Ji, P. J.; Atherton, J. H.; Page, M. I. *Faraday Discuss.* **2010**, *145*, 15.

DOI: 10.1021/acs.joc.5b02794
J. Org. Chem. 2016, 81, 1635−1644

(33) Ji, P.; Atherton, J.; Page, M. I. *Org. Biomol. Chem.* **2012**, *10*, 5732.
(34) Diraison, M.; Martyna, G. J.; Tuckerman, M. E. *J. Chem. Phys.* **1999**, *111*, 1096.
(35) Ricci, M. A.; Nardone, M.; Ricci, F. P.; Andreani, C.; Soper, A. K. *J. Chem. Phys.* **1995**, *102*, 7650.
(36) Bunnett, J. F.; Morath, R. J. *J. Am. Chem. Soc.* **1955**, *77*, 5051.
(37) Bernasconi, C. F. *J. Am. Chem. Soc.* **1970**, *92*, 129.
(38) Chéron, N.; El Kaïm, L.; Grimaud, L.; Fleurat-Lessard, P. *Chem. - Eur. J.* **2011**, *17*, 14929.
(39) Błaziak, K.; Mąkosza, M.; Danikiewicz, W. *Chem. - Eur. J.* **2015**, *21*, 6048.
(40) Błażej, S.; Mąkosza, M. *Chem. - Eur. J.* **2008**, *14*, 11113.
(41) Szpakiewicz, B.; Grzegozek, M. *Russ. J. Org. Chem.* **2004**, *40*, 829.
(42) Frisch, M.; Trucks, G.; Schlegel, H.; Scuseria, G.; Robb, M.; Cheeseman, J.; Scalmani, G.; Barone, V.; Mennucci, B.; Petersson, G. *Gaussian 09*; Gaussian, Inc.: Wallingford, CT, 2010.
(43) Zhao, Y.; Truhlar, D. G. *Theor. Chem. Acc.* **2008**, *120*, 215.
(44) Hehre, W. J.; Radom, L.; Schleyer, P. v. R.; Pople, J. A. *Ab Initio Molecular Orbital Theory*; Wiley: New York, 1986; Vol. *33*.
(45) Fukui, K. *Acc. Chem. Res.* **1981**, *14*, 363.
(46) Hratchian, H. P.; Schlegel, H. B. *J. Chem. Phys.* **2004**, *120*, 9918.
(47) Hratchian, H.; Schlegel, H. *J. Chem. Theory Comput.* **2005**, *1*, 61.
(48) Goossens, H.; Vervisch, K.; Catak, S.; Stankovic, S.; D'hooghe, M.; De Proft, F.; Geerlings, P.; De Kimpe, N.; Waroquier, M.; Van Speybroeck, V. *J. Org. Chem.* **2011**, *76*, 8698.
(49) Stankovic, S.; Catak, S.; D'hooghe, M.; Goossens, H.; Tehrani, K. A.; Bogaert, P.; Waroquier, M.; Van Speybroeck, V.; De Kimpe, N. *J. Org. Chem.* **2011**, *76*, 2157.
(50) Catak, S.; Monard, G.; Aviyente, V.; Ruiz-Lopez, M. F. *J. Phys. Chem. A* **2009**, *113*, 1111.
(51) D'hooghe, M.; Van Speybroeck, V.; Van Nieuwenhove, A.; Waroquier, M.; De Kimpe, N. *J. Org. Chem.* **2007**, *72*, 4733.
(52) Catak, S.; Monard, G.; Aviyente, V.; Ruiz-Lopez, M. F. *J. Phys. Chem. A* **2006**, *110*, 8354.
(53) Van Speybroeck, V.; Moonen, K.; Hemelsoet, K.; Stevens, C. V.; Waroquier, M. *J. Am. Chem. Soc.* **2006**, *128*, 8468.
(54) Hutter, J.; Iannuzzi, M.; Schiffmann, F.; VandeVondele, J. *Wiley Interdisciplinary Reviews: Computational Molecular Science* **2014**, *4*, 15.
(55) Becke, A. D. *Phys. Rev. A: At., Mol., Opt. Phys.* **1988**, *38*, 3098.
(56) Lee, C.; Yang, W.; Parr, R. G. *Phys. Rev. B: Condens. Matter Mater. Phys.* **1988**, *37*, 785.
(57) Goedecker, S.; Teter, M.; Hutter, J. *Phys. Rev. B: Condens. Matter Mater. Phys.* **1996**, *54*, 1703.
(58) Grimme, S.; Antony, J.; Ehrlich, S.; Krieg, H. *J. Chem. Phys.* **2010**, *132*, 154104.
(59) Lin, I. C.; Seitsonen, A. P.; Tavernelli, I.; Rothlisberger, U. *J. Chem. Theory Comput.* **2012**, *8*, 3902.
(60) Ensing, B.; Klein, M. L. *Proc. Natl. Acad. Sci. U. S. A.* **2005**, *102*, 6755.
(61) Van Houteghem, M.; Ghysels, A.; Verstraelen, T.; Poelmans, W.; Waroquier, M.; Van Speybroeck, V. *J. Phys. Chem. B* **2014**, *118*, 2451.
(62) Del Ben, M.; Hutter, J.; VandeVondele, J. *J. Chem. Phys.* **2015**, *143*, 054506.
(63) Bussi, G.; Donadio, D.; Parrinello, M. *J. Chem. Phys.* **2007**, *126*, 014101.
(64) Fujisaki, H.; Moritsugu, K.; Matsunaga, Y.; Morishita, T.; Maragliano, L. *Front. Bioeng. Biotechnol.* **2015**, *3*, 125.
(65) Roe, D. R.; Bergonzo, C.; Cheatham, T. E. *J. Phys. Chem. B* **2014**, *118*, 3543.
(66) Sutto, L.; Marsili, S.; Gervasio, F. L. *Wiley Interdisciplinary Reviews: Computational Molecular Science* **2012**, *2*, 771.
(67) Laio, A.; Parrinello, M. *Proc. Natl. Acad. Sci. U. S. A.* **2002**, *99*, 12562.
(68) Laio, A.; Gervasio, F. L. *Rep. Prog. Phys.* **2008**, *71*, 126601.
(69) Moors, S. L. C.; De Wispelaere, K.; Van der Mynsbrugge, J.; Waroquier, M.; Van Speybroeck, V. *ACS Catal.* **2013**, *3*, 2556.
(70) Van der Mynsbrugge, J.; Moors, S. L. C.; De Wispelaere, K.; Van Speybroeck, V. *ChemCatChem* **2014**, *6*, 1906.
(71) Limongelli, V.; Bonomi, M.; Parrinello, M. *Proc. Natl. Acad. Sci. U. S. A.* **2013**, *110*, 6358.
(72) Jónsson, H.; Mills, G.; W, J. K. In *Classical and Quantum Dynamics in Condensed Phase Simulations*; Berne, B. J., Ciccotti, G., Coker, D. F., Eds.; World Scientific: Singapore, 1998.
(73) Bolhuis, P. G.; Chandler, D.; Dellago, C.; Geissler, P. L. *Annu. Rev. Phys. Chem.* **2002**, *53*, 291.

DOI: 10.1021/acs.joc.5b02794
J. Org. Chem. 2016, 81, 1635−1644